



A comparative study of piscine defense: The scales of *Arapaima gigas*, *Latimeria chalumnae* and *Atractosteus spatula*



Vincent R. Sherman^a, Haocheng Quan^a, Wen Yang^b, Robert O. Ritchie^c, Marc A. Meyers^{a,d,*}

^a Department of Mechanical and Aerospace Engineering, Materials Science and Engineering Program, University of California San Diego, La Jolla, CA 92093, USA

^b Department of Materials, ETH Zurich, 8093 Zurich, Switzerland

^c Department of Materials Science and Engineering, University of California Berkeley, CA 94720, USA

^d Department of Nanoengineering, University of California San Diego, La Jolla, CA 92093, USA

ARTICLE INFO

Keywords:

Scales
Bioinspiration
Bouligand
Alligator gar
Coelacanth
Arapaima

ABSTRACT

We compare the characteristics of the armored scales of three large fish, namely the *Arapaima gigas* (arapaima), *Latimeria chalumnae* (coelacanth), and *Atractosteus spatula* (alligator gar), with specific focus on their unique structure-mechanical property relationships and their specialized ability to provide protection from predatory pressures, with the ultimate goal of providing bio-inspiration for manmade materials. The arapaima has flexible and overlapping cycloid scales which consist of a tough *Bouligand*-type arrangement of collagen layers in the base and a hard external mineralized surface, protecting it from piranha, a predator with extremely sharp teeth. The coelacanth has overlapping elasmoid scales that consist of adjacent *Bouligand*-type pairs, forming a double-twisted *Bouligand*-type structure. The collagenous layers are connected by collagen fibril struts which significantly contribute to the energy dissipation, so that the scales have the capability to defend from predators such as sharks. The alligator gar has inflexible articulating ganoid scales made of a hard and highly mineralized enamel-like outer surface and a tough dentine-like bony base, which resist powerful bite forces of self-predation and attack by alligators. The structural differences between the three scales correspond with the attack of their predators, and show refined mechanisms which may be imitated and incorporated into superior bioinspired and biomimetic designs that are specialized to resist specific modes of predation.

1. Lessons from natural dermal armors

Nature has produced an extraordinary number of unique and specialized materials over hundreds of millions and even billions of years of evolution. For thousands of years natural designs have provided inspiration for manmade structures, such as ancient armors. However, it is only in recent times that humans have come to realize that studying, understanding, and mimicking these materials may serve as an important route for the design and development of new specialized synthetic materials. Despite being comprised of only a limited palette of constituents with relatively modest mechanical properties, biological materials can exhibit remarkable combinations of strength, toughness and reliability that are crafted through ingenious designs involving hierarchical assemblies and gradients in composition, structure and properties. This has stimulated many studies throughout the world to seek to understand biological materials and the mechanisms that are responsible for their functions, *e.g.*, Sacks and Sun (2003), Meyers et al. (2008), Ji and Gao, 2010 and Chen et al.

(2012). As the principles underlying the properties of biological materials become clarified, they can be applied to the development of new materials. Two recent examples include a bioinspired glass, produced by Chintapalli et al. (2014), which mimics natural designs to display exceptional toughness, and freeze-cast bioinspired anisotropic ceramic scaffolds produced by Porter et al. (2012) as a refinement of a synthesis method developed by Deville et al. (2006) and Munch et al. (2008). Unfortunately, there are not too many current examples of successful bioinspired *structural* materials and processing them can be extremely complex (Wegst et al., 2015). However, advancements in manufacturing are opening new and exciting opportunities, and the development of a bioinspired, synthetic flexible armor is a goal worth pursuing.

With regards to natural dermal armor, fish scales are a common example and have been the subject of much research, particularly over the past decade. They are an intriguing topic because they have provided effective protection to fish for eons; some armored fish have existed prior to the dinosaurs, which came into existence 225 million

* Corresponding author at: Materials Science and Engineering Program, University of California, San Diego, CA 92093, USA.
E-mail address: mameyers@ucsd.edu (M.A. Meyers).

years ago. The fish scales have been traditionally classified into four groups: placoid, elasmoid, cosmoid and ganoid. Placoid scales are denticles with a flattened rectangular base plate embedded in the fish body, and spines which project from the posterior surface. They have a core with pulp which is surrounded by dentine and an outer vitrodentine layer. Cosmoid scales are similar to placoid scales and likely evolved from the fusion of them; they have dentine, vitrodentine and a tissue complex known as cosmine with interconnected canals and flask-shaped cavities, but lack a pulp core. These rigid rhombic scales are now, unlike the other scale classifications, entirely extinct. Ganoid scales are modified cosmoid scales which are also rhombic, rigid, and jointed articulating scales of two layers. A thin mineral surface layer called ganoine replaces the vitrodentine, and lies atop a bony foundation which replaces the cosmine. Peg and socket joints often join ganoid scales. Elasmoid scales likely evolved from ganoid scales and are the most common among living vertebrates. They are thin and imbricate, resembling shingles on a roof, and consist of a bony surface and a fibrous layer beneath of collagen. There are two subcategories, ctenoid and cycloid, the difference between being that ctenoid scales have developed surface spines which are bony and grow from the body of the scale to the surface and the cycloid scales have a smooth surface (Sire and Huysseune, 2003; Helfman et al., 2009; Sire et al., 2009; Vickaryous and Sire, 2009).

Each of these scales has unique features and provides protection with a modest weight penalty. In order to learn from natural fish scales, modern tools and techniques, such as electron microscopy, nano-indentation, computer x-ray tomography and finite element analysis, provide insight into the features at the nano to macro level and reveal a variety of toughening mechanisms that make fish armors highly effective. Early studies on fish scales of this nature include *Polypterus senegalus* (Bruet et al., 2008; Song et al., 2011), *Morone saxatilis* (Zhu et al., 2013), *Arapaima gigas* (Torres et al., 2008; Lin et al., 2011) and *Atractosteus spatula* (Allison et al., 2013; Yang et al., 2013).

One principal function of fish scales is to resist penetration from predators. In particular, the manner in which they resist pressure by teeth has been addressed by several researchers. Zhu et al. (2012) performed penetration tests on a *Morone saxatilis* (striped bass) fish scale using a steel stylus simulating a sharp tooth. They compared the force-penetration response of whole fish scales and just the collagen layer with that of the synthetic polymers and found marked differences. By analyzing the penetration sequence in the bony surface and collagenous foundation, they classified it into three stages: stage I represents a linear relationship between force and penetration distance due to flexing of the scale and penetrating into the surface bone layer. Stage II begins with a small force drop associated with the crack opening in the bone layer and radiating from the penetration point which finally propagates into the collagen layer. In stage III the force-displacement curve plateaus as the stylus punctures the collagen layer. In similar vein, Vernerey and Barthelat (2010) described the load

redistribution mechanisms (proportional to scale size) from penetration on the overlapped fish scales (Fig. 1a). They also described relationships between scale density, ratio of angular attachment stiffness to bending stiffness, and a variety of other properties which are key to the scales' protective function (Fig. 1b) and vary according to the environment in which the fish lives. If escaping from a predator is critical, the structure of fish scale is "designed" in terms of flexibility (strain stiffening) and lightness; if the protection from a predator is more important, higher resistance to fracture and average bending stiffness are design criteria. Similarly, characterizing the structure, quantifying the mechanical parameters and understanding the salient mechanisms can provide insight to understand the environment in which the fish exist, the types of predators the fish may have faced, and even aids in understanding the evolution of the fish.

In this review, we focus on the three resilient fish (Fig. 2) whose highly effective dermal armors have protected them survive for millions of years, namely *Arapaima gigas* (arapaima) (Torres et al., 2008; Lin et al., 2011; Zimmermann et al., 2013), *Latimeria chalumnae* (coelacanth) (Roux, 1942; Smith et al., 1972), and *Atractosteus spatula* (alligator gar) (Allison et al., 2013; Yang et al., 2013), with an emphasis on the structure-mechanical property relationships in their respective armored scales. It has been established that the properties of fish scales may vary with the head, body, and tail having unique traits (Marino Cugno Garrano et al., 2012; Murcia et al., 2015), but this case there is no knowledge of what specific part of the animal they are from; this may lead to some experimental variation. The arapaima is a huge fish which lives in the Amazon and grows upwards of 3 m in length and 200 kgf in weight (National Geographic, 2016a). Its fossil records have remained the same for at least 23 million years, and it evolved in order to peacefully cohabitate with the piranha, a predator with famously sharp tricuspid teeth with a tooth tip radius of 13 μm . Despite its ferocity, the piranha possesses a relatively small bite force, estimated by Meyers et al. (2012) as 20 N. The coelacanth is another large fish which lives at up to 700 m deep in the Indian ocean (specimens have been found in the Madagascar and Indonesian coasts), and grows to 2 m in length and 90 kgf in weight. It has existed for 400 million years, and was thought to have gone extinct with the dinosaurs until rediscovered in 1938 (Smith, 1939). Shark bite marks found on coelacanths suggest that the shark is one possible predator (Fricke et al., 1991). Shark teeth are nearly as sharp as the piranha's, with a 16 μm tooth edge radius, but different types of sharks possess biting forces ranging between 1–2400 N (Huber et al., 2009; Mara et al., 2010; Ferrara et al., 2011). The bite force of sharks is surprisingly low, and this is understandable because they do not possess bones and only cartilage. Finally, the alligator gar is a third large fish which lives in the brackish waters around the Gulf of Mexico and grows up to 3 m and 140 kgf (National Geographic, 2016b). The gar has existed in its current form for roughly 100 million years, and must protect itself from alligators. The alligator has 80 teeth although it may generate 3000 over its life (Potts, 1998), but these teeth which are not

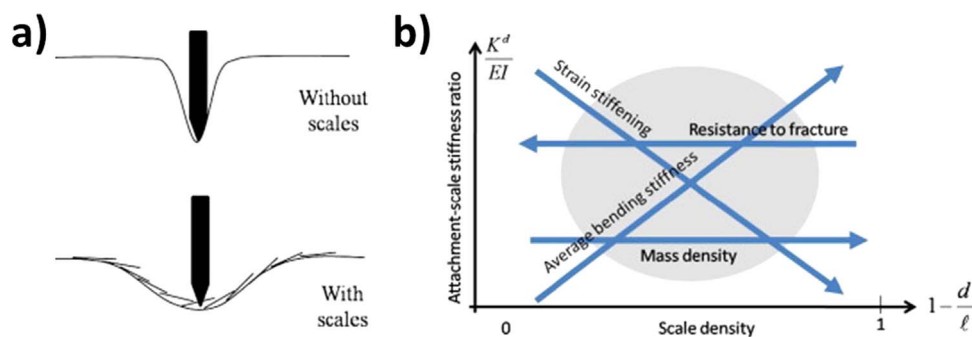


Fig. 1. (a) Scales redistribute an applied load in a region proportional to the scale size. This also leads to a greater penetration resistance. (b) Plot of attachment to scale stiffness ratio as a function of scale density illustrates several relationships between scale properties and features of the response such as average bending stiffness, resistance to fracture, and mass density (from Vernerey and Barthelat (2010)).

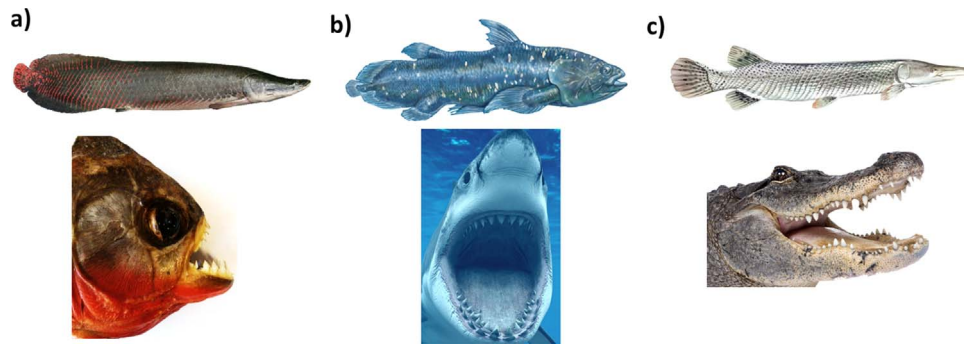


Fig. 2. Ruthless predators and their prey. (a) The piranha is an infamously ferocious fish which cohabitates with the arapaima in the Amazon; the arapaima grows up to 3 m in length and 180 kgf in weight. (b) The shark is suspected to be the main predator of the coelacanth, which can grow to over 2 m in length and 90 kgf in weight. (c) The alligator, known for its massive jaw strength and powerful attacks, cohabitates the Mississippi basin with the alligator gar, a fish which grows up to 3 m in length and 140 kgf in weight.

particularly sharp, have a tip radius of the order of $\sim 80\text{--}130\ \mu\text{m}$ for juveniles up to 3 mm for adults. This lack of sharpness, however, is compensated by powerful jaws capable of bite forces of 10 N to 10 kN, depending on the size (Erickson et al., 2003; Erickson et al., 2004).

2. Arapaima gigas

2.1. Structure of arapaima scales

As shown in Fig. 3, the arapaima fish has elasmoid scales (cycloid as the sub-classification) which are composed of a hard and stiff outer mineral layer and a tough lamellar *Bouligand*-like collagen structure beneath. The scales are overlapped and arranged with a degree of imbrication (exposed length/total length) equal to 0.4 and aspect ratio (length/thickness) of 50 (Yang et al., 2014). The average number of scale layers covering the fish's body is three, and the darker parts of the scale are exposed while the light parts are overlapped by surrounding scales (Fig. 3). The exposed scale is covered by a thick mineral layer ($\sim 1\ \text{mm}$ in adults) with ridges on the surface; in the embedded portion of the scale the mineral layer is thinner ($\sim 0.5\ \text{mm}$). Beneath the mineral, collagenous lamellae display a *Bouligand*-type structure, involving large ($\sim 45\text{--}90^\circ$) angles between adjacent layers. Individual lamella consists of parallel and straight collagen fibrils, although there is significant misorientation between the fibril directions in adjacent lamellae. Fibrils can be imaged by transmission electron microscopy (TEM), as shown in Fig. 3, where the misorientation between the two visible lamellae is visible. The cross-section of fibrils in layer 1 of collagen is elliptical and the periodicity of the banding in collagen

fibrils in layer 2 is $\sim 50\ \text{nm}$, *i.e.*, less than the 67 nm characteristic d period of collagen. This indicates that the fibrils are at an angle to the surface, which can be calculated as $\theta = \arccos(50/67) \sim 40^\circ$, and that the included angle between the two layers is less than 90° .

2.2. Mechanical response of arapaima scales

Owing to the large overlap area over the entire fish, the flexibility of each individual scale is a requirement for the mobility of the arapaima. As such, its scales are flexible in all directions, a characteristic of all elasmoid scale classifications as compared to ganoid scales, such as those of the alligator gar. When these scales are tested in tension in the longitudinal and transverse directions (Fig. 4a), with the mineral layer either intact or removed, there is a substantial decrease in the strength with the mineral layer present. This decrease is associated with the mineral's inability to carry tensile load due to the presence or formation of microcracks, *i.e.*, the outer mineral layers merely increase the cross-sectional area and correspondingly decrease the stress. Although the arapaima fish scale is flexible in all directions, the scale in the longitudinal direction, *i.e.*, along its length, is stiffer (0.5 vs. 0.2 GPa) and stronger (25–50 vs. 15–20 MPa) than in the transverse direction (Yang et al., 2014). The stronger and stiffer direction of the scale aligns with a possible extendon function of the scales, where scales store energy for more efficient swimming (Brainerd, 1994). The more compliant direction allows the scales to accommodate movement as they conform to the curvature of the fish body. However, as previously addressed, the specific location of the scales on the fish is unknown and this effect may vary throughout the fish.

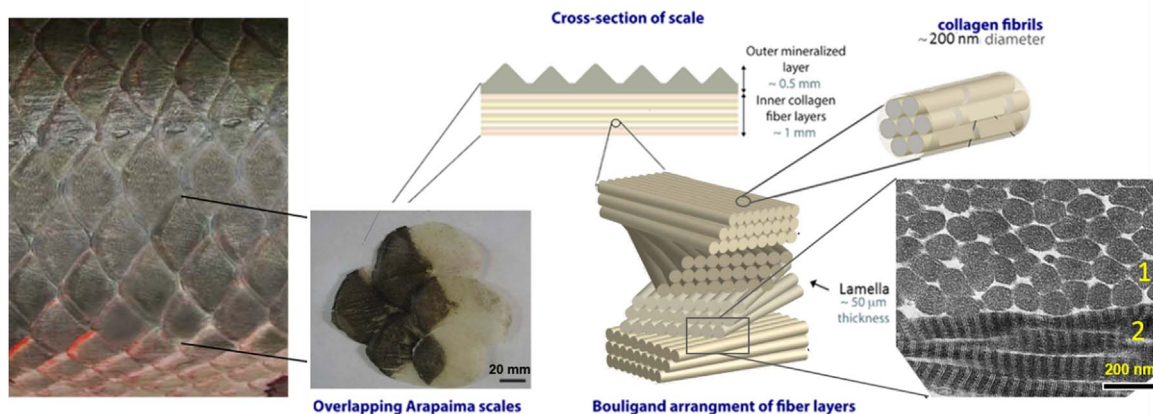


Fig. 3. Structure of the scale of *Arapaima gigas*. The arapaima's elasmoid scale has a hierarchical structure which is designed to defend against piranha attacks. The underlying shape of the scales can be seen in the overlapping arrangement schema of five scales. The exposed portion of the scale is dark and consists of mineral ridges atop a *Bouligand*-type lamellar base of collagen, creating the cross-section shown. The white part of the scale is covered by surrounding scales, and consists of the same *Bouligand* layers as beneath the mineral ridges. These collagen layers are made of sheets of oriented collagen fibrils, roughly 200 nm in diameter and with some degree of mineralization; two layers of differing orientations are observable in the TEM micrograph (adapted from Zimmermann et al. (2013) and Yang et al. (2014)).

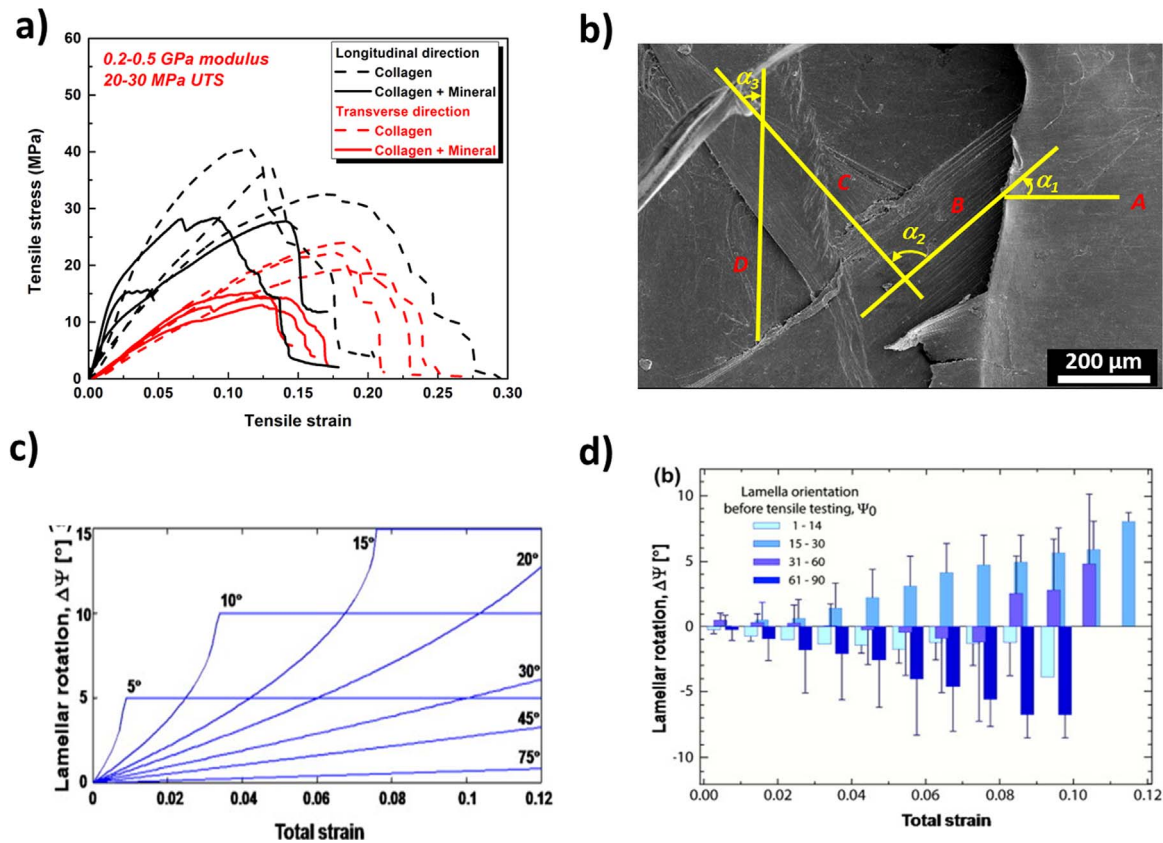


Fig. 4. Mechanical response and lamellar rotation of the arapaima scale. (a) The tensile response of the arapaima scale is characterized by elastic and plastic regions (Yang et al., 2014). The tensile response of the scales shows that they are weaker when the mineral layer is not removed, due to the fact that the mineral is brittle and microcracks defeat its strength. (b) The variation in lamellar orientation is not consistent between layers. Three orientations of adjacent layers are shown; two at acute angles and one at an obtuse angle. (c) The lamellar reorientation of these layers can be predicted mathematically based on their initial orientation using Eq. (1). The plotted results show that under load, all layers should reorient towards the tensile axis, but those layers with the strongest tendency are those oriented roughly 10–30° from the tensile axis. (d) The lamellar reorientation predicted from (c) is measured experimentally using SAXS. (from Yang et al. (2014) and Zimmermann et al. (2013)).

Scanning electron microscopy (SEM) shows that the lamellar angles are large and variable (Fig. 4b), and are arranged in a *Bouligand*-type structure, which is highly resistant to crack propagation. Under tensile loading, some lamellae reorient as the deformation is applied so that the lamellae close to the tensile axis can more effectively carry the applied load. This reorientation has been estimated theoretically by considering the elastic stretching, strain-rate sensitivity and interfibrillar sliding of the lamellae (Zimmermann et al., 2013; Yang et al., 2014):

$$\Psi_1 - \Psi_0 = \arccos \left[\frac{\cos \Psi_0 (\epsilon_t + 2)}{2 + C \left(\frac{\dot{\epsilon}}{\dot{\epsilon}_0} \right) \frac{\epsilon_t}{E_f}} \right], \quad (1)$$

where Ψ_1 is the predicted angle between the lamella and the tensile axis (positive values correspond to rotation towards the tensile axis), Ψ_0 is the initial value of Ψ before the application of the load, ϵ_t is the sum of the strain due to the elastic stretching of fibrils and rotation with the effect of interfibrillar shear, $\dot{\epsilon}$ is the strain rate, $\dot{\epsilon}_0$ is a reference strain rate, E_f is the modulus of a fibril, and C is an experimentally measured constant. Predictions from Eq. (1) for the angular rotation shown in Fig. 4c indicate that all orientations will rotate towards the tensile axis, with the most significant reorientation occurring for Ψ angles between 10° and 30°. Corresponding experimental measurements of the scales, under tensile loading with real time small angle x-ray scattering (SAXS) imaging, provide a detailed observation and analysis of the mechanisms in Fig. 4d. SAXS results indicate that under tensile loading, the collagen fibrils oriented to within ~15–30° of the

loading direction tend to rotate towards the tensile axis, whereas fibrils in the 61–90° range rotate away from the tensile axis. Owing to the large angles between layers, as the collagen fibrils oriented close to the loading direction rotate towards it, the adjacent layers, which are far from the tensile axis are subjected to tension perpendicular to the fibrils, causing gaps to open. In addition, interfacial shear and sympathetic lamellar rotation by adjacent layers contribute to these orientations, on average, rotating away from the tensile direction (Yang et al., 2014).

2.3. Arapaima failure prevention strategies

The arapaima can effectively defend against piranha attacks due to the highly mineralized, hard surface layer of its scale, and a *Bouligand*-type structure of the layer beneath. The mineral layer resists the penetration by a tooth, and the *Bouligand* foundation provides strength and toughness to accommodate the deformation. The damage evolution in the scale, and its corresponding toughness, have been examined by tensile testing notched specimens of the scale *in situ* in the SEM (Yang et al., 2014). Fig. 5 shows a sequence of images captured during such tests: at the beginning of the tensile test, fibrils at the notch tip start to delaminate in the vicinity of the notch tip (Fig. 5a). Under increasing load, the collagen fibrils become stretched, with some fracturing close to the notch tip, while other fibrils away from the tip become curved due to the geometry of notch-opening and the rotating from the layers beneath (shown in Fig. 5b). Before fracture, more collagen fibrils delaminate (labeled as 1 in Fig. 5c), some fracture (labeled as 2), bend or buckle (labeled as 3), but other layers remain intact and carry the load (labeled as 4 in Fig. 5c,d). Similarly, Dastjerdi

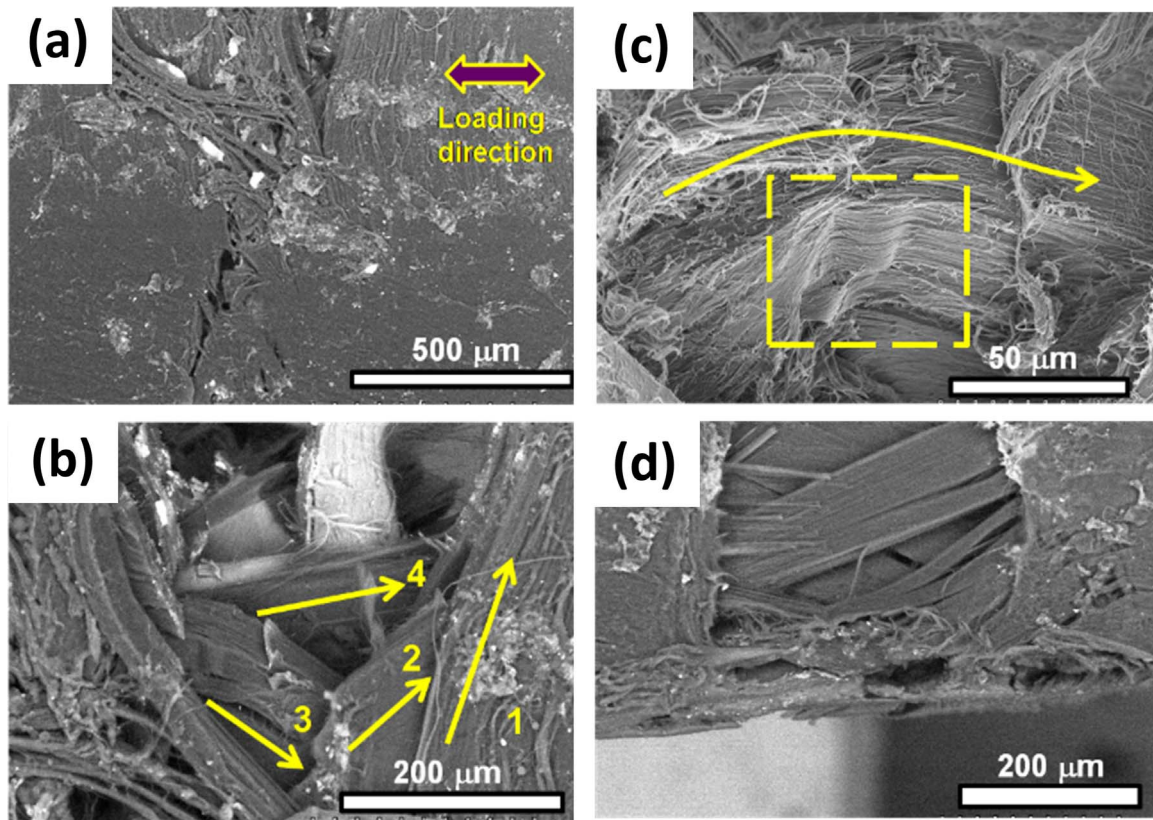


Fig. 5. *In situ* SEM of a crack arrested in arapaima scales under tensile loading. (a) An initially notched scale is loaded in tension in the direction indicated. (b) As stretching continues, multiple layers become apparent as lamellae stretch, reorient, bend, and buckle. (c) Lamellar delamination occurs as an energy absorbing mechanism. (d) The crack is fully arrested by reorientation, bending and stretching of the layers (from Yang et al. (2014)).

and Barthelat (2015) measured the fracture toughness of striped bass scales (also an elasmoid scale) and found them to be among nature's toughest materials ($J_c=15\text{--}18\text{ kJ m}^{-2}$). The scales negate the effect of cracks as they effectively delocalize into wide process zones with the partially detached collagen fibers engulfing the crack front.

To further assess the effectiveness of arapaima scales, Meyers et al. (2012) examined how an actual piranha tooth can penetrate the arapaima scale. With the tooth mounted on the upper fixture of the testing machine so that it could be compressed into hydrated arapaima scales, it fractured before complete perforation of the scales occurred (Fig. 6). The images show the sequence of events (for the tooth and the scale) during the test, with a picture of the failed tooth as an inset to the force-displacement plot. Microscopically, the lamellar base of the scales was observed and shown to serve as a resilient and tough base which acts synergistically with the hard and stiff outer mineral layer to prevent penetration from the tooth. Hence, this highly effective armor allows the passive arapaima to cohabitate peacefully with the piranha, one of the most vicious and feared fish in the Amazonian waters.

3. *Latimeria chalumnae*

3.1. Structure of coelacanth scales

The coelacanth has an ancient type of elasmoid scales, which were present several times during the fish evolution. (Fig. 7). Similar to cycloid scales, these scales have a dark region with a rough and more mineralized exposed surface, and an overlapped (embedded) region of which the surface is light and smoother. The individual scales have an elliptical shape with various sizes corresponding to the size of the fish and they are typically $\sim 10\text{--}35\text{ mm}$ in size for a 1 m fish. The degree of imbrication is ~ 0.34 and the aspect ratio is ~ 55 , similar to the arapaima. These scales provide protection by means of a highly

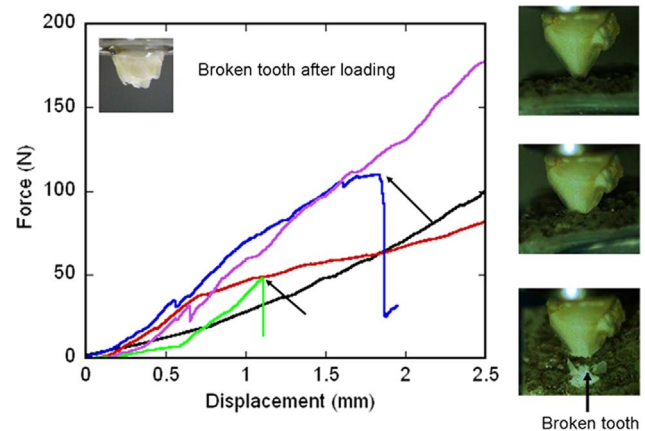


Fig. 6. Piranha tooth penetration of the arapaima scale. During an indentation experiment, the piranha tooth attempts to fully penetrate a single arapaima scale. A sequence of images on the right shows a time evolution of the penetration. The protective mineral and lamellar *Bouligand* structure base causes tooth fracture before the scale can be fully penetrated. The fracture of the tooth is indicated by the drop in force as seen in the force vs. displacement measurement (identified by black arrows) and the broken tooth is pictured as an inset within the graph (from Meyers et al. (2012)).

mineralized outer layer with unique “double-twisted” *Bouligand* foundation (Giraud et al., 1978). The surface of embedded region is shown in Fig. 7b. From the center of the scale circular annular ridges with various spacings can be observed. Additional ridges radiating from the center are initially perpendicular to the annuli and then orient towards the dorsal-lateral direction. These ridges, shown in Fig. 7c, have a spacing of approximately $30\text{ }\mu\text{m}$. On the surface of the exposed region, denticles protrude from the scale towards the direction of the fish tail (Fig. 7d). The mineral layer is needed for protection, although Sudo

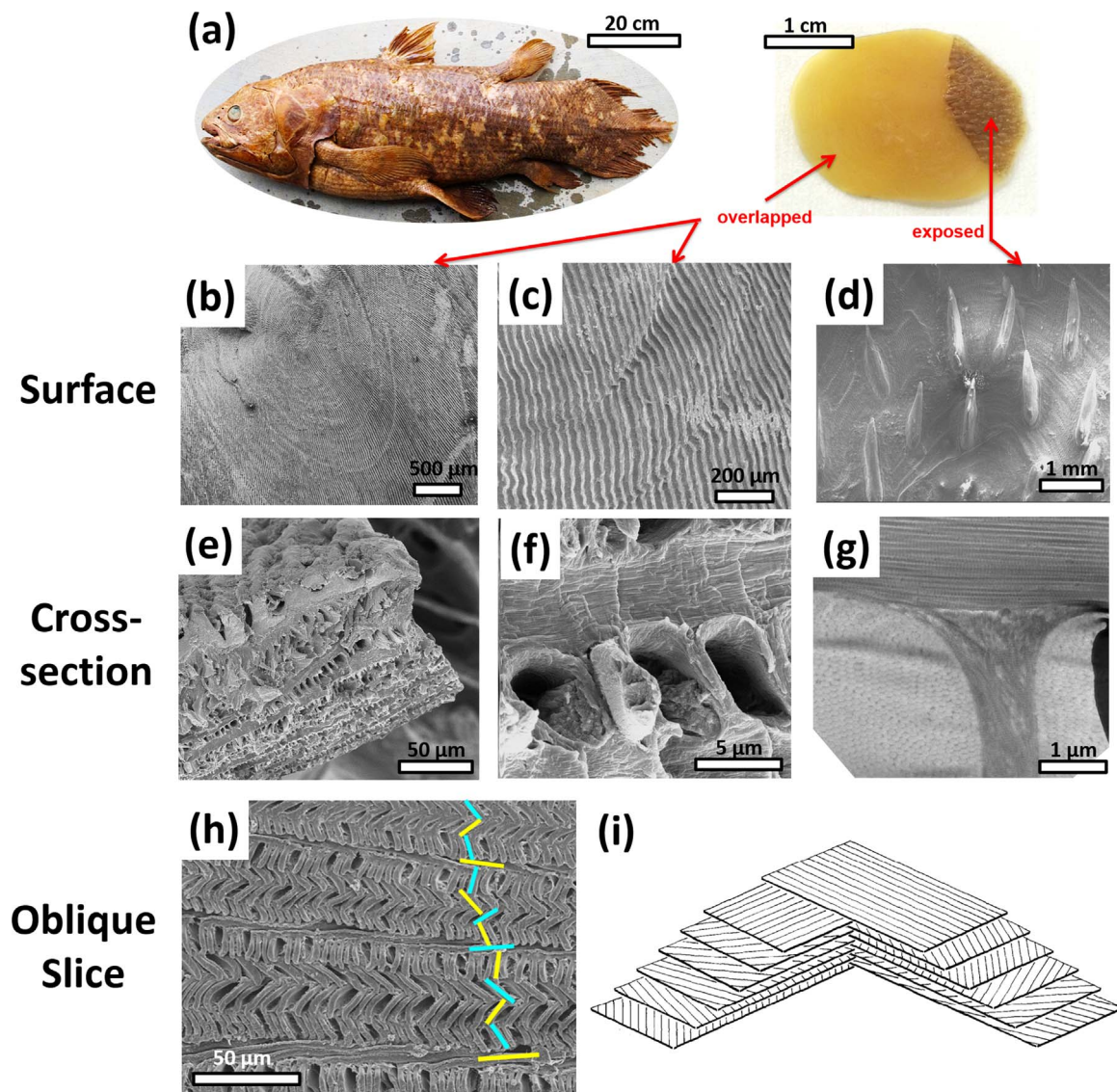


Fig. 7. Overview of the scale of coelacanth. (a) The entire body of coelacanth is covered by elasmoid scales. (b) The scales are oblong and the complete surface of the scale is comprised of stacked layers, which originate at the intersection of the exposed and covered portions of the scale. A ridge at the edge of each oval layer transitions to the layer beneath. (c) Each layer has comb-like ridges which radiate from the center of the scale. (d) The exposed portion of the scale has denticles which angle towards the tail of the fish. (e) Cross-sectional view of the scale shows the internal collagenous lamellae. (f) SEM and (g) TEM of adjacent lamellae the collagenous struts connecting them. (h) An oblique cross-section shows the change in orientation of adjacent layers. (i) The progression of layers and orientations shown schematically (from Giraud et al. (1978)).

et al. (2002) studied the scales of the *Sebastes inermis* (rockfish), which also has ctenoid scales, and showed the surface roughness aligns with the direction of the water current and serves to channel flow for a hydrodynamic advantage.

Beneath the rough and hard exposed surface, the majority of the scale thickness is composed of collagenous lamellae, identified as isopedine (Goodrich, 1907; Ørving, 1957; Smith et al., 1972; Giraud et al., 1978). Isopedine is also present in the ganoid scales of Senegal bichir (Bruet et al., 2008). The laminated structure of the coelacanth scale is shown in Fig. 7e. The lamellae in the isopedine have two superimposed and interpenetrating *Bouligand* structures with a remarkably regular arrangement in which the parallel fibers in any one lamella lie at a roughly 90° angle to the fibers in adjacent lamellae (Fig. 7i) (Smith et al., 1972; Giraud et al., 1978). The architecture of the coelacanth scale differs from the arapaima scales, as they have struts with less ordered collagen fibrils connecting the lamellae and filling the gaps between collagen bundles. Fig. 7f shows holes in the scale cross-section which indicate that the collagenous bundles “pull-out” when the sample is fractured. Transmission electron microscopy

of these scales (Fig. 7g) shows aligned collagen fibrils along the lamellae and less organized fibrils in the struts, forming a continuous network. The orientation of lamellae can be readily identified from the oblique slice shown in Fig. 7h. The fibril directions are marked and show that the orientations of the collagen lamellae in adjacent layers are nearly orthogonal, while successive bilayers are characterized by a clockwise rotation of ~30° (when observing from the top of the figure down). This arrangement, first described by Giraud et al. (1978) and subsequently termed “double twisted”, is illustrated schematically in Fig. 7i, which shows the collagen orientation in each odd layer and each even layer (including the rotation between the layers), and how the combination of the two *Bouligand* structures forms the double twisted structure.

3.2. Mechanical response of coelacanth scales

The pseudo-orthogonal ‘plywood’ structure of the isopedine of the coelacanth scales leads to in-plane isotropy, with no significant difference between the mechanical responses along longitudinal and

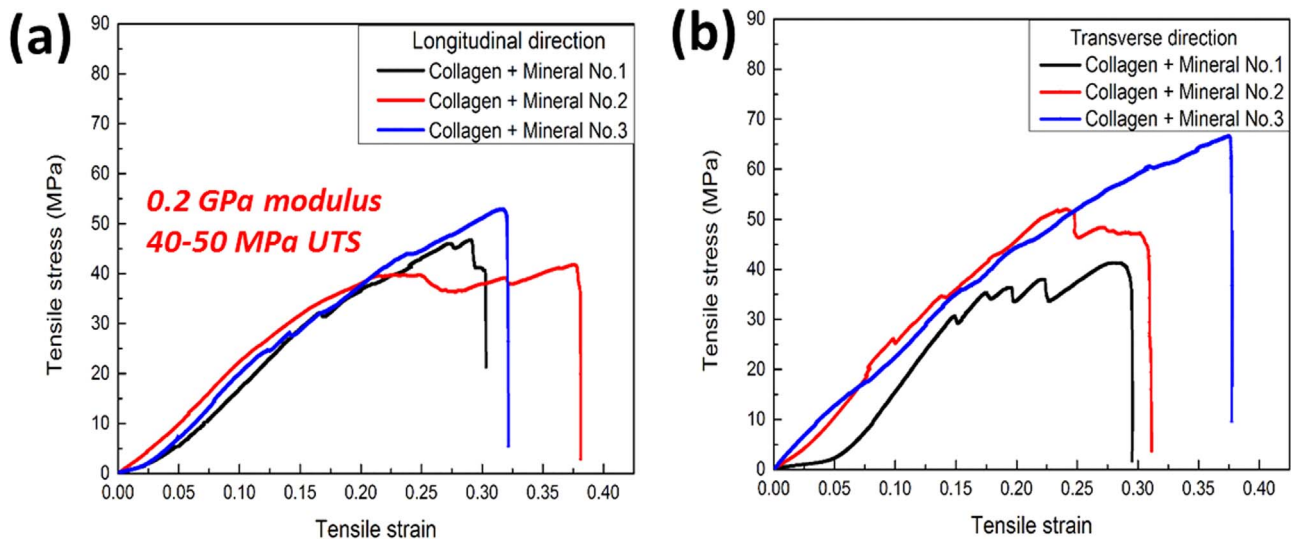


Fig. 8. Mechanical response of the coelacanth scale. Comparison of the tensile stress as a function of strain for the coelacanth scales in (a) the longitudinal and (b) the transverse direction. The in-plane isotropy results from the periodic relationship between lamellae; the lamellae are oriented as two interpenetrating *Bouligand* structures (ABAB) where the A and B orientations are perpendicular to one another and subsequent AB pairs are twisted by $\sim 30^\circ$ with respect to the previous pair. This structure promotes strength as well as isotropy; the relatively strong scales have an ultimate tensile strength between 40 and 50 MPa.

transverse directions. Tensile stress-strain curves, shown in Fig. 8a and b, reveal a Young's modulus in the longitudinal direction of ~ 210 GPa with a tensile strength of ~ 50 MPa, as compared to respective values of ~ 250 GPa and ~ 50 MPa along transverse direction. This in-plane 'isotropic' mechanical response is substantially different from the mechanical response of arapaima scales, which have higher strength and stiffness in the longitudinal direction. The work-of-fracture in coelacanth scales (area under the stress-strain curve) before complete fracture is about 10 MJ m^{-3} in both longitudinal and transverse

directions. This is much higher than the work-of-fracture in arapaima scales, which is $1\text{--}2 \text{ MJ m}^{-3}$. This indicates that the role of collagen struts between the lamellae is important and provides additional deformation ability to the structure, contributing significantly to the toughness of these scales.

3.3. Coelacanth failure prevention strategies

Fig. 9a and b shows the extension of a crack in a pre-notched

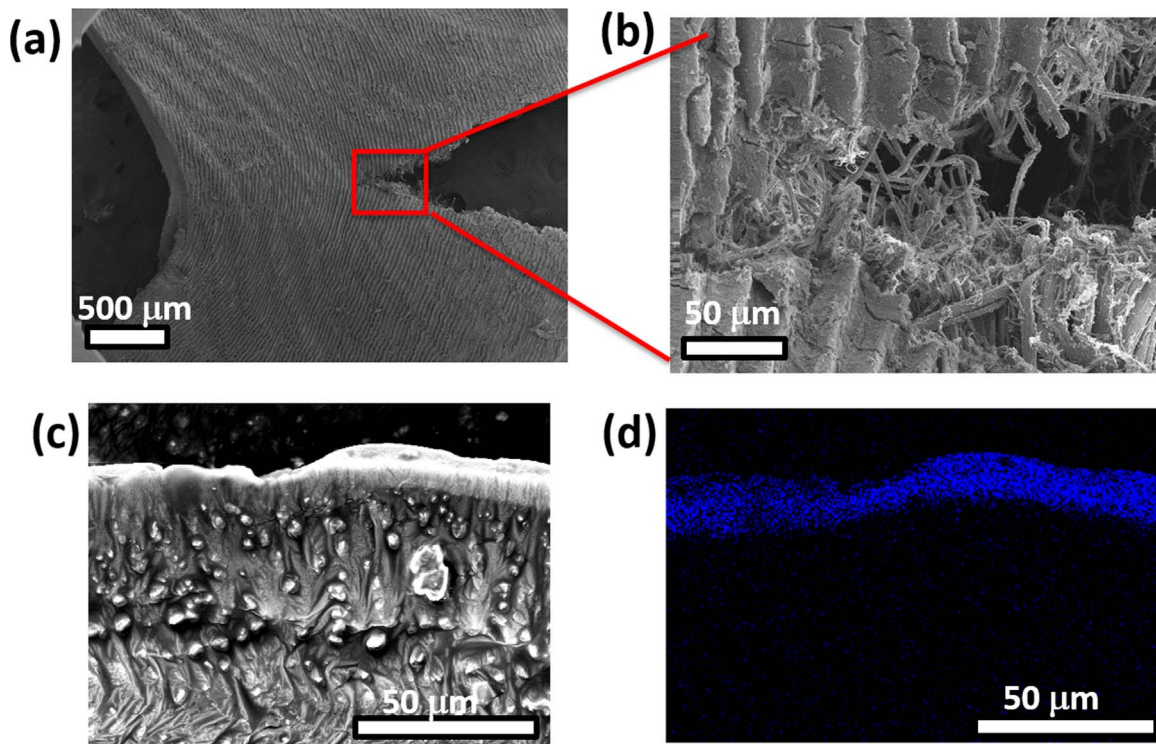


Fig. 9. Crack arrested by the collagen fibrils and EDX image of outer layer of coelacanth scale. (a) A notched tensile test is paused to illustrate the opening of the scale during tensile crack propagation. (b) Expanded view of crack tip demonstrating extensive bridging of the crack by collagen fibers and blunting of the crack tip. Individual lamellae are not visible, but a large amount of collagen fiber pullout and complete lamellar delamination are the key energy absorbing features. (c) SEM of the cross-section of the scale used for energy dispersive x-ray analysis (EDX). (d) EDX shows high mineral content of outer surface as well as a small amount of mineral distributed in the scale indicated by the blue features. The black area corresponds to low mineral content.

coelacanth scale. As the crack propagates, the collagen fibers form bridges in front of the main crack front and delocalize failure. Thus, the crack tip becomes blunted by collagen fibrillary bridging, similar to that shown in striped bass scales (Vernerey and Barthelat, 2014). Fig. 9c shows the highly mineralized surface layer (top); element mapping of calcium in Fig. 9d indicates that this outer layer of the scale has much higher mineralization than the inner layer.

To examine how these scales defend against an attack by the coelacanth's predator, the shark, a shark's tooth is attached to a load frame and penetrated through two scales, with fish flesh placed underneath to mimic the coelacanth body. The force vs. displacement curve in Fig. 10 shows two drops as the tooth penetrates through the two scales. The penetration of one coelacanth scale occurs at approximately 15 N (the first drop in the curve) and 25 N for the subsequent scale, which is inferior to the arapaima scale that can withstand loads in excess of 100 N.¹ As potential predators of the coelacanth, sharks with ~ 70 teeth (depending on the species) may have a bite force of up to 2400 N (blacktip shark: 420 N; horn shark: 200 N; hammerhead shark: 2400 N; bullshark: 1000 N as summarized by Mara et al. (2010)). The bite force is distributed across a number of teeth, although in some cases (especially with larger sharks) the scales would be expected to suffer penetration. The coelacanth scales would successfully defend from many smaller sharks, but inevitably the fish would fall victim to the more powerful sharks in the ocean. For this reason, the fish's ability to remain hidden (Fricke et al., 1991) is crucial to its survival.

4. *Atractosteus spatula*

4.1. Structure of alligator gar scales

The alligator gar scales provide protection from alligators as well as from self-predation. Sharp teeth are not a major concern, as in the case for other fish, but the gar's defense must be effective in resisting the powerful bite force and impact of ambush predators. The fish has ganoid scales characterized by a hard enamel-like mineral layer and a dentine-like foundation consisting of a bony composite of collagen and mineral. In the living fish, the scales are not exposed but are covered by a layer of skin (Daget et al., 2001). Fig. 11a shows the scales without the outer skin layer. The ganoin layer (white in image, green in micro-computed tomography (μ -CT) scan in Fig. 11b) covers most of the surface of the scale, while the overlapped region is the bony foundation (yellow in image, red in μ -CT). Fig. 11a shows the shapes and organization of the gar scales, where three types of scales are required to provide full coverage of the fish. Type I is the most common type of scales and cover most of the gar. Type II scales are found where rows of Type I scales converge, and Type III scales are found at the extremities of the fish. The edges of the Types I and III scales may have serrated ridges which serve to cut predators as the fish thrashes and are shown by the arrow in Fig. 11b. The scales on the fish form an imbricated array; the reported aspect ratio is 8.66 and the degree of imbrication is 0.78 (Yang et al., 2013) which is much larger than for the arapaima (0.4) and coelacanth (0.34) and is a result of a small overlap region. This highlights a major difference between the gar and most other fish: it is protected principally by only one layer of scales, although this is also the case for the ganoid scales of the Senegal bichir (Bruet et al., 2008). In the overlap regions the thickness of the scale is reduced so that adjacent scales fit to produce a constant thickness. These chamfered overlapping edges provide protection against penetration when the tooth tip impinges on the boundary. The advantage of a small overlap area is to minimize weak interfaces at the junctions of scales,

¹ Penetration distances measured in the testing machine are a function of both the actual scale penetration and compression of the foundation beneath; as such, these distances cannot be compared across the three fish.

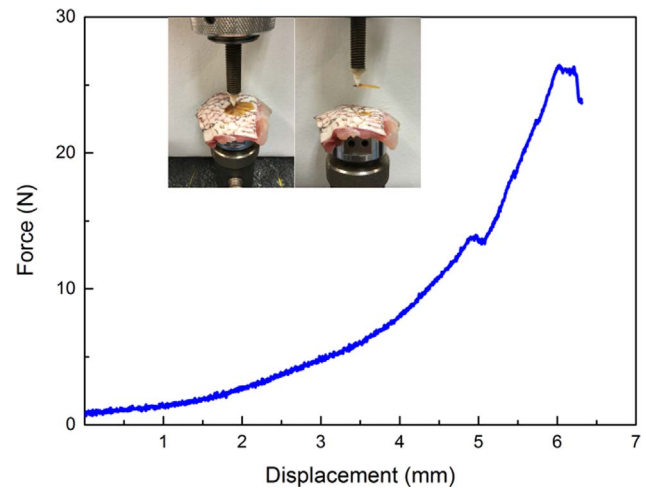


Fig. 10. Penetration of a coelacanth scale by a shark tooth. Two overlapped scales are penetrated in the exposed area by a shark tooth. The arrangements of the coelacanth scales are such that the covered portion of a second scale exists immediately below exposed surfaces. The force displacement diagram indicates that penetration and damage of the scale is possible due to the shark's bite force; the two drops in load correspond to visible penetration of the shark tooth through two scales.

while still permitting the mobility of the fish, as ganoid scales are much stiffer than the scales of either the arapaima or the coelacanth and do not readily flex during fish movement. The ganoine, shown in Fig. 11c, consists of distinct layers of decussated mineral in a crossed pattern, while in the bony layer, shown in Fig. 11d, hollow tubules and fibrils (the head of a single fibril is shown in the inserted picture) are present which run throughout the thickness of the scale (Fig. 11e).

4.2. Mechanical response of alligator gar scales

The main predator of the alligator gar is the alligator whose bite force can range from 10 N to 10 kN (Erickson et al., 2003; Erickson et al., 2004). Both the bite force and the radius of the tooth tip increase with the mass of the predator. Thus the natural design of alligator gar scale is to have stiff and strong fish scales with minimal overlap, where connective tissue ensures the linkage as well as flexibility. The principal function of the rigid scales is to resist the high forces by delocalizing them. Fig. 12 shows compressive and tensile stress-strain curves of the bony region of the gar scale. Results for the orientation perpendicular to the scale surface (orientation A) are in black, with blue and red lines for the orientation parallel to the surface plane of the scale, but perpendicular (orientation B) and parallel to the serrated edge (orientation C), respectively. The average compressive strength and failure strain perpendicular to the surface are 300 MPa and 0.3, respectively, and the two in-plane directions are 210 MPa and 240 MPa with maximum strain values of 0.17 and 0.25, respectively. The ultimate strength and failure strain perpendicular to the scale are significantly different from these properties in the two in-plane directions, specifically because the tubules and fibrils run normal to the scale surface, or from the interior to outer surface of the scale. In a previous study, Yang et al. (2013) reported moduli for these scales: 5.4–6.0 GPa for dry scales and 4.8–5.5 GPa for wet ones (obtained by compression results). In contrast, the elastic moduli measured using nanoindentation showed far less variation: 10.0 GPa when wet and 10.9 to 13.2 GPa when dry. The latter tests probe a far smaller region of the scale which is likely to be uniform, whereas the compressive tests on ~2-mm sized cubes of bulk material sample a much larger volume of the scale and probe its heterogeneous nature with flaws and pores, all of which lead to a reduction of stiffness. The ultimate strength and failure strain perpendicular to the scale are significantly different from these properties in the two in-plane directions, specifically because the tubules and fibrils run in the direction normal to the scale surface, or

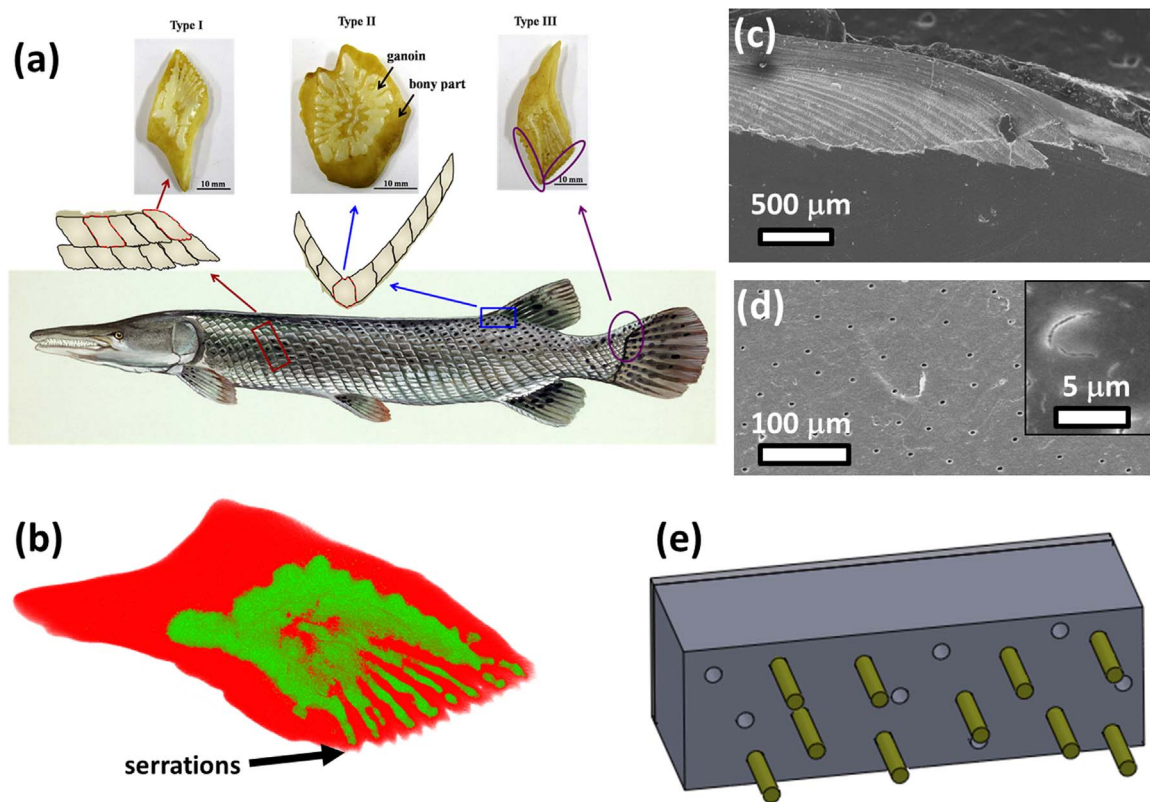


Fig. 11. Structure of the scales of *Atractosteus spatula*. (a) The protective armor is formed of three principal types of scales, shown as type I, II, III. The outer surface of the scale is covered with a layer of dermis. Below and in direct contact with the dermis, some portions of the scale are covered with ganoine, a white colored enamel-like mineral. The darker areas around the ganoine are a bone-like composite of protein and mineral; these areas correspond to the portions of the scales that are directly overlapped by surrounding scales. (b) These two regions are easily visualized using micro-computed tomography; in the scan shown the green is indicative of the dense ganoine mineral, while the red indicates the bony composite. (c) The two regions and their interface are shown. A saw tooth interface is observed, as well as clearly defined mineral layers. The surface of the ganoine is characterized by small rounded reliefs called tubercles. (d) The bony region of the scale has hollow tubules and collagen fibrils which run throughout. (e) The arrangement of these is demonstrated by a schematic which shows the ganoine (outer layer) and the bony inner layer with tubules (hollow) and collagen (green) dispersed throughout. (For interpretation of the references to color in this figure legend, the reader is referred to the web version of this article.)

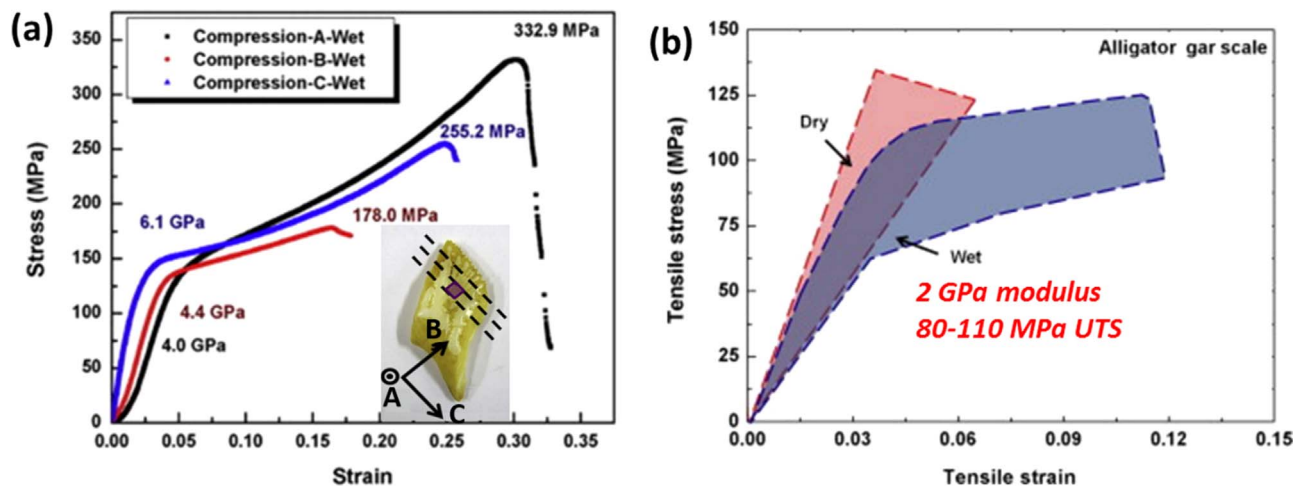


Fig. 12. Mechanical response of alligator gar scale. (a) The compressive response of the bony region of the alligator gar scale. Differences between orientations are due to the orientation of mineral and tubules in the scale. (b) The tensile response of the alligator gar scale. Dry scales have a linear response while hydrated scales have a bilinear response due to the plasticity induced by the presence of water; in the dry state, hydrogen cross-linking creates strong bonds between all components, while in the hydrated state weaker hydrogen bonds are formed with water molecules which allow plasticity as these bonds are broken and reformed (from Yang et al. (2013)). (For interpretation of the references to color in this figure legend, the reader is referred to the web version of this article.)

from the interior to outer surface of the scale. However, there appears to be no structural features which would lead to dissimilar responses in the plane of the scale.

The difference between the properties of the scale when wet or dry can also be seen by the tensile data for the longitudinal direction (Fig. 12b). Interestingly, both wet and dry scales show similar stiffness

and strength. Typically both free convection dehydration and dehydration through the introduction of a polar solvent result in an increase in inter-peptide hydrogen bonds which, although weaker in strength, result in stiffening and strengthening due to the increase in quantity (Murcia et al., 2016). However, this effect may be interrupted by high amounts of mineralization, which is why the strength and stiffness in

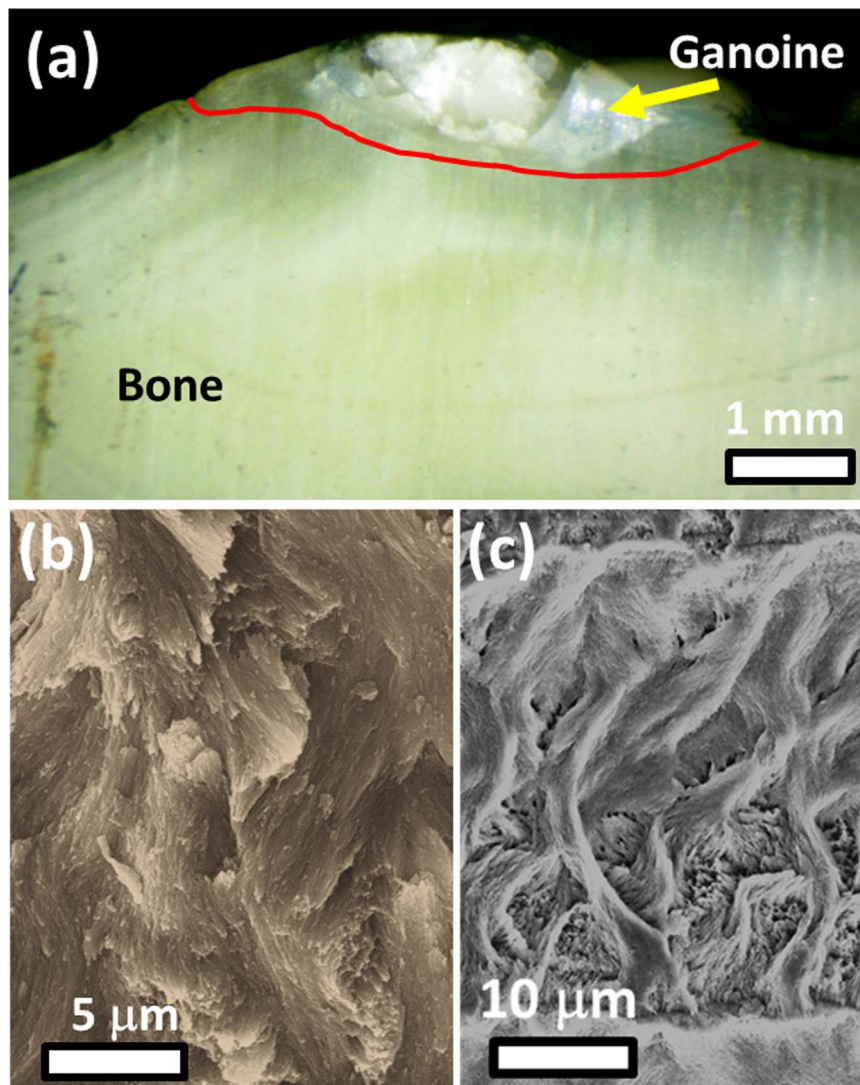


Fig. 13. Failure aversion of the alligator gar scale by mineral decussation. (a) Compressive failure of the mineral layer (the separation between mineral and bone is shown by the red line). (b,c) The arrest of incipient cracking is due in part to the enamel-like weaving of the mineral, called decussation, which the ganoine exhibits. This decussation is observed on a mineral fracture surface (b) and by use of an etchant (c). Both show the woven structure with mineral texture protruding towards the outer scale surface, which appears to be even more extreme than the weave of tooth enamel. The etchant also clearly reveals distinct mineral layers which are indistinguishable in a fracture surface.

the highly mineralized alligator gar scale are similar when wet and when dry. The critical difference is the post-yield behavior in the wet scales which display extensive plasticity, due to the breaking and reforming of hydrogen bonds between water molecules and collagen fibrils (Maciel et al., 1996). Such plasticity is clearly important to the mechanical properties, especially the toughness of the gar scale. In tension, the dry scales do not exhibit significant plasticity. However, the compressive tests show a bi-linear response. This may be associated with a much greater difficulty in opening cracks in compression. Fig. 12b shows the curves in tension, with the absence of plasticity. Dry and wet fish scales are toughened by differing mechanisms which are addressed in the following section.

4.3. Alligator gar failure prevention strategies

The alligator gar has a variety of refined features and strategies which aid in protection against attack, as described in detail by Sherman et al. (2016). First, the outer mineral layer (Fig. 13) has an arrangement of crystals which greatly contributes to the toughness of the ganoine. Fig. 13a shows cracks which initiate in the ganoine layer under compressive load yet arrest within the layer; this prevents cracks from propagating into the bony layer to cause failure of the scale. The

mineral bundles in ganoine, observed from both a fractured surface (Fig. 13b) and polished and etched surface (Fig. 13c), are shown to be twisted and interlocked with other bundles, in a manner similar to that seen in tooth enamel (Bajaj and Arola, 2009). This decussation, or cross-plyed arrangement of crystals, guides the cracks along a tortuous path through the twists and turns of the mineral, requiring significantly more energy to propagate.

Another important feature of the alligator gar scales are the tubules in the inner layer that are oriented nearly perpendicular to the scale surface. These tubules provide channels for vascular flow and the delivery of nutrients. Fig. 14a shows a single tubule and the fracture surface (Fig. 14b) shows the tubules and collagen fibers in the structure, confirming that they are nearly parallel. The tubules can cause crack meandering when the scale is dry (Fig. 14d) which would increase the toughness of the scale by up to a factor of two for in-plane deflections. However, the scales of the fish are not dry and this effect does not appear to occur when the scales are hydrated (Fig. 14c). This begs the question as to whether the tubules contribute to the *in vivo* fracture resistance of the alligator gar scale. The water molecules can act as a plasticizer and enhance plastic deformation and ductility in the wet scale, which we believe is the principal toughening mechanism in the presence of water; this is shown in Fig. 12b. Finite element

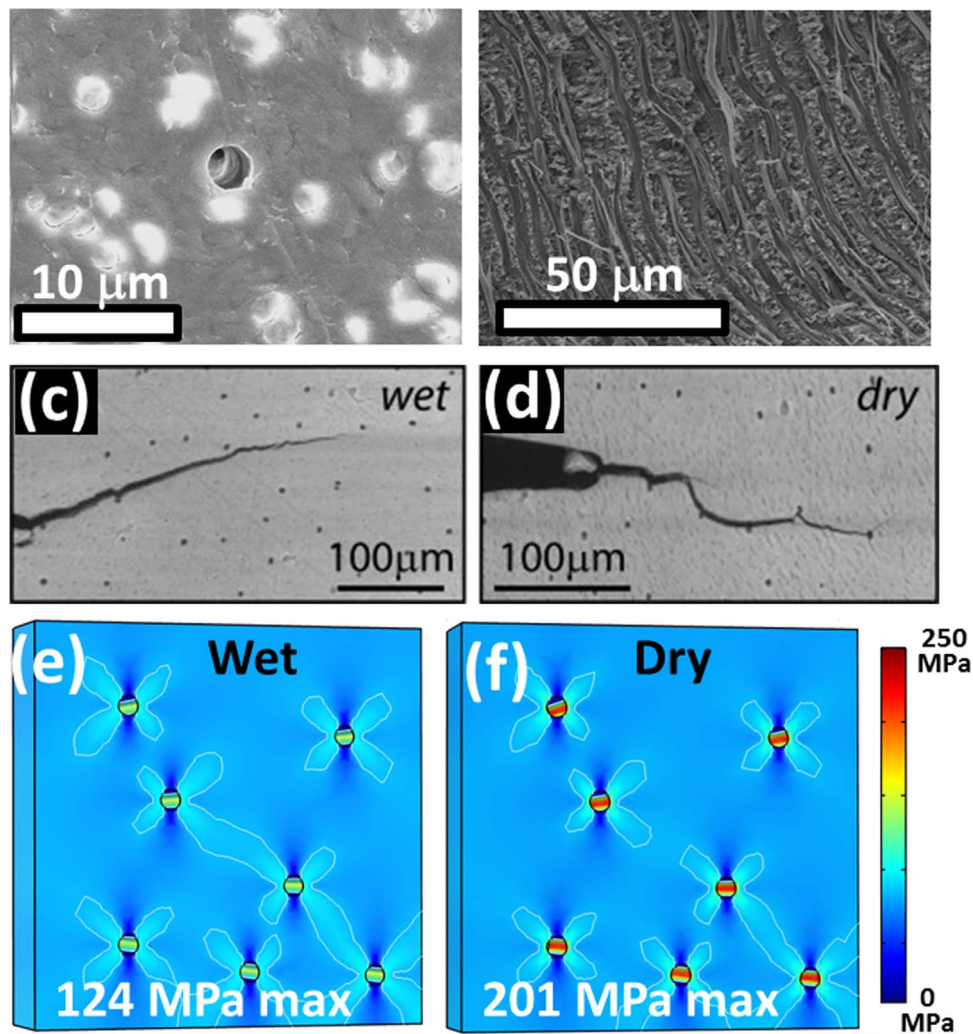


Fig. 14. Failure aversion of the alligator gar scale by tubule effects. (a) High magnification view of tubule and surrounding collagen fibril heads. (b) Fracture along tubule and fibril direction shows parallel and regularly spaced fibrils. (c) When wet, tubules have little influence on the crack propagation. (d) When dry, the tubules cause crack meandering as the crack deflects from tubule to tubule. (e and f) Finite element simulations of an applied load of 70 MPa applied to dry (linear elastic) and wet (elastoplastic) scales. Contour lines are drawn at 77 MPa. (e) The plasticity of the hydrated tensile response leads to a decrease in the stress around tubules and more homogenous stress distribution. This decrease in stress corresponds with an increase in localized strain. (f) The dry scale experiences significantly higher stresses around tubules, and inhomogeneous stress distribution with clear directions of high stress which the cracks follow, causing crack meandering.

modeling was performed in COMSOL. The constitutive equations used in the FEM analysis are based on the two responses given in Fig. 12b, and dry scales were modeled as a linear elastic solid while wet scales were modeled as an elastoplastic solid. These results confirm that the plasticity in the wet scale acts to markedly diminish the stress concentrations around the tubules by almost a factor of two, making the stress distribution far more even throughout the scale. This allows increased strain values to be achieved, and enhances the absorption of strain energy (Fig. 14e and f).

The effectiveness of the gar scale array is demonstrated by experiments involving the penetration of an alligator tooth shown in Fig. 15. A foam pad was placed beneath the scales to simulate the flesh of the fish. Application of pressure caused adjacent scales to hinge on one another in order to resist from penetration. Small concentric cracks occurred in the ganoine layer, but were arrested and did not propagate or cause failure. Eventually, at a force of ~500 N, the alligator tooth failed, illustrating the capability of the gar scale to withstand the high forces from the predatory action of an alligator. Tooth failure under the alligator's biting force is because in an actual bite, the force of up to 10 kN is distributed among the ~80 teeth in an alligator's mouth. The radius of the adult tooth tip is much larger (~up to 3 mm) and the load at which the tooth fracture would be significantly increased.

5. Comparison of the three fish scales

The arapaima, coelacanth and alligator gar scale have different predators, and comparing the mechanical properties with the structural characterization as well as the toughening mechanisms which were described in the previous sections provides insights on the armor suited for different applications. Key features of the three types of scales being compared are presented in Table 1. The relative hardness and stiffness of the three fish scales, calculated using micro- and nano-indentation measurements, are plotted in Fig. 16. Although the hardness and stiffness of these scales are different for each fish because of their specific protective requirements, they are all designed with the concept of a hard and stiff outer surface with a relatively soft and tough foundation to accommodate excessive damage. Beyond this common design principle, each scale has a specialized structure which corresponds to the specific mechanisms providing a competitive advantage over their predators, which have been discussed above. These mechanisms of protection against predators have clearly been successful as they have enabled these fish to survive for millions of years.

To compare the three fish scales and their defense capability, predator tooth sharpness, predator bite force as well as the modulus of the fish scales are summarized in Fig. 17. To give a clear comparison,

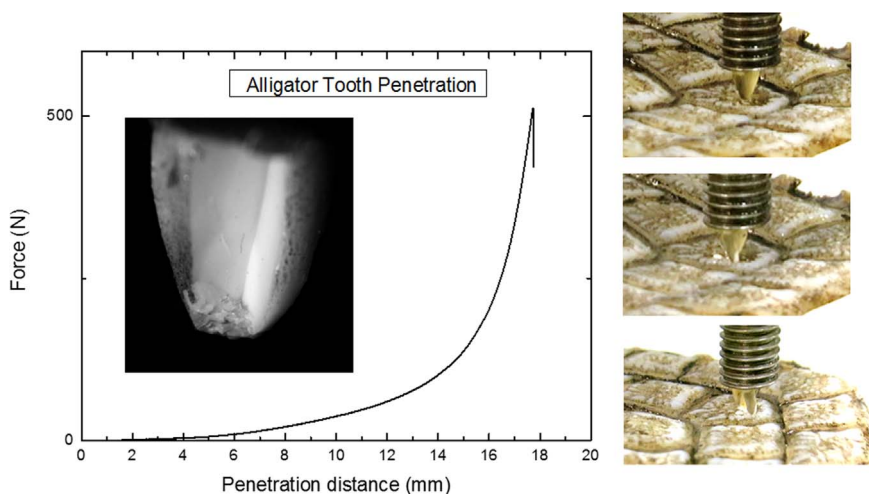


Fig. 15. Penetration of an alligator gar scale array by an alligator tooth. As pressure is applied, the scales hinge at their interfaces in order to absorb and conform to the flexing (overlapped scales redistribute penetration load over a larger area). As the test continues, the tooth breaks at 500 N, which corresponds to the maximum force in the plot. The scales are sufficiently strong to resist the high applied force from one tooth (biting force distributed to ~80 teeth) and defeat the attempted penetration by an alligator tooth. The inset shows the fractured tooth after an “attempted attack”.

values are normalized by maximum values. It is clear that minimal overlap (and corresponding large degree of imbrication) of systems with stiff scales, such as alligator gar, can defend against a predator with a large bite force but a large radius of the teeth tips. However, facing predators with sharp teeth (small tip radius) requires more flexible scales with large overlap regions (consistent to a low degree of imbrication).

6. Bioinspired flexible armor

Inspiration from nature in the design of armor has existed since the days of the Roman Empire. The *lorica squamata* mimicked lizard skin and provided protection to the soldiers while ensuring mobility. Indeed, the name squama signifies “scales” in Latin. The plates of *Lorica squamata* were 0.5–1 mm thick and had dimensions of 15–25 mm across, similar to the arapaima and coelacanth. These scales provided the best protection, superior to *Lorica segmentatata* (metal lamellar hoops associated with Roman legionnaires in movies), and *Lorica hamata* (chain mail). *Lorica squamata* was superior because the majority of the body was covered by two plates in which the kinetic energy of projectiles was transferred laterally.

Researchers are currently using new techniques to mimic the overlap system of the fish scales as well as specification of the aspect ratio and imbrication in order to tune the flexibility and protection function of future bioinspired armor. Rudykh et al. (2015) investigated the resistance to penetration of a microstructured elasmoid scale-inspired armor. Indentation and bending tests on bioinspired 3-D printed structures, shown in Fig. 18a and b, optimized protection against penetration and flexibility, amplifying penetration resistance by a factor of 50 while reducing flexibility by less than a factor of 5. This was achieved by identifying and separately analyzing the mechanisms which govern flexibility and penetration resistance. Similar efforts by Funk et al. (2015) have led to the creation of a synthetic “fish skin” for the production of soft materials through a combination of a mesh or dermis-like layer and rigid scales. The assembled product is not specific

to any particular classification of fish scale, but incorporates components that are key to the armor’s mechanical response. The resulting assembly, shown in Fig. 18c and d, is flexible, lightweight, transparent, and robust under mechanical load. It is claimed to have a potential application as a thin protective coating for soft materials. It is also important to understand how a stiff plate performs on a soft substrate; Martini and Barthelat (2016a) showed that small plates may fail by tilting due to a localized force, and emphasized the importance of avoiding this dangerous failure mode which drastically reduces the effectiveness of stiff armor plates. Additionally, Martini and Barthelat (2016b) produce a bioinspired armor shown in Fig. 18e and f, made of ceramic tiles and a soft substrate and capable of a large degree of flexibility and also resistant to penetration.

Another unique biological feature learned from the arapaima scale is that of the concept of “flexible ceramics”. This refers to the ability of the collagenous foundation of the scales to flex without damaging the mineralized surface (Meyers et al., 2012), as shown in Fig. 18g and h, which allows arrangements of larger scales to retain flexibility. The tensile strains at the bottom of the mineralized ridges are considerably lower than those encountered if the mineralized layer had a homogeneous thickness. Correspondingly, localized cracking occurs at the bottom of the ridges but is much less damaging. Rudykh and Boyce (2014) similarly demonstrated that super flexible composites may be produced with an elasmoid scale type arrangement, using a large volume fraction of the stiff phase in order to promote protection with little compromise in flexibility.

Recent studies have targeted the design of armor plates inspired from the architecture of the alligator gar scale. These armored plates, 3-D printed with ABS and machined using zirconia, simplify the geometry of the gar scale into an easily manufactured shape which retains its primary features to allow for exceptional flexibility and penetration resistance with little compromise between the two. To achieve this, an exceptionally hard and inflexible articulating unit hinges on adjacent units through matching radii of curvature using arrays of additively manufactured ABS and machined zirconia tiles in

Table 1

Comparison of the properties of arapaima, coelacanth, and alligator gar scales.

Fish	Aspect ratio	Imbrication degree	Mineral content	Structure	Ultimate tensile strength	Tensile modulus	Nano-indentation modulus
Arapaima	50	0.4	43%	Bouligand	15–40 MPa	200–500 MPa	1.3 GPa to 0.5 GPa
Coelacanth	55	0.34	53%	Double-twisted Bouligand	50 MPa	200 MPa	0.5 GPa to 0.2 GPa
Alligator gar	8.66	0.78	65%	Bone and enamel	90–115 MPa	2 GPa	3.7 GPa and 0.75 GPa

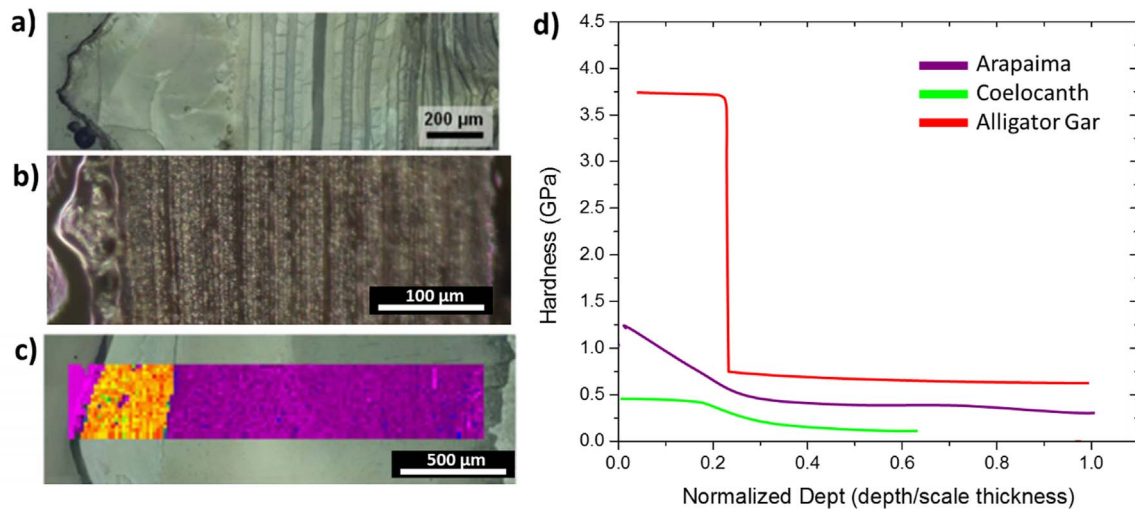


Fig. 16. Nanoindentation and microindentation of the cross-sections of scales. (a) Nanoindentation of the arapaima scale shows that the surface mineral has a hardness of ~1.3 GPa; the hardness decays with decreasing mineral to a value of ~0.5 GPa in the *Bouligand*-type foundation. (b) The coelacanth scale has a nanoindentation hardness of ~0.5 GPa in the mineral layer which, similar to the arapaima, continuously decreases to ~0.2 GPa as mineral content decreases. (c) The alligator gar scale has a nanoindentation hardness of ~3.7 GPa in the mineralized ganoine outer surface; a sharp transition between the outer surface and the boney base causes an immediate hardness decrease to ~0.75 GPa. (d) Hardness *vs.* normalized depth plots of across each of the three scales reveal harder outer surfaces and softer foundations.

the image of gar scales (Fig. 19). Fig. 19a–c shows the initial production of ABS scales, and their ability to flex and retain coverage. Fig. 19d is the next iteration of the model with zirconia tiles mounted on Kevlar in order to retain the crucial flexibility with much improved protection.

7. Conclusions

In this paper, we have reviewed the armored scales of three large fish: the *Arapaima gigas* (arapaima), *Latimeria chalumnae* (coelacanth) and *Atractosteus spatula* (alligator gar). Each of these fish utilize a different class of scales for protection, respectively cycloid, ctenoid, and ganoid. These finely tuned dermal armors have protected these fish for millions of years, and barring direct or indirect human intervention, will likely continue to do so. Like most armors, these scales are designed with a hard outer surface to resist penetration and a tough inner foundation to accommodate excessive strains. However, each type of scale owes its effectiveness to specific features which are related to the fish's main predators:

- The elasmoid (cycloid) scale of the arapaima enables flexibility in spite of a highly mineralized exposed surface and substantial overlap to effectively resist the penetration of piranha teeth. The ridges on the surface enable the mineral to effectively flex, minimizing the tensile stresses acting on it.
- The elasmoid (ctenoid) scale of the coelacanth has a much lower stiffness but higher ultimate strength (40–60 MPa) than that of the arapaima (30 MPa), with a considerably higher work-of-fracture (9–10 MJ m⁻³ *vs.* 1–1.5 MJ m⁻³). Although the coelacanth scale uses similar mechanisms to the arapaima, the interfibrillar collagen struts between the collagen bundles in the structure contribute significantly to the energy dissipation.
- The ganoid scale of the alligator gar resists the extreme bite forces of its predators by having a highly mineralized, tough and strong foundation beneath a hard and stiff ganoine outer layer. The wet gar scales dissipate energy as the water molecules act as a plasticizer to promote ductility while in the dry scales the tubules provide toughening through crack deflection and meandering.

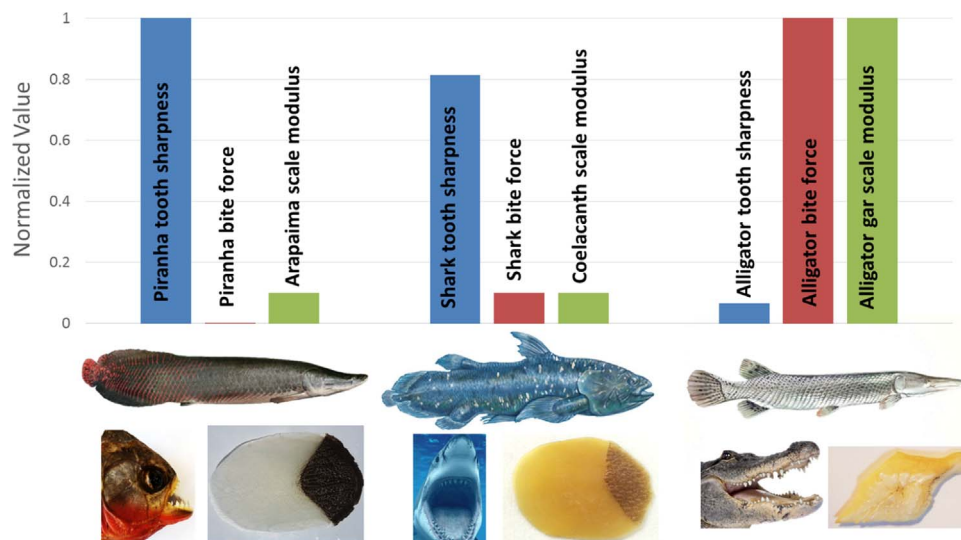


Fig. 17. Comparison of normalized predator tooth sharpness, predator bite force, and prey scale modulus. The high imbrication of stiff alligator gar scales can defend against predators with large bite forces and dull teeth (large tooth tip radius), while the more flexible scales of the coelacanth and arapaima can defend against sharp teeth (small tooth tip radius).

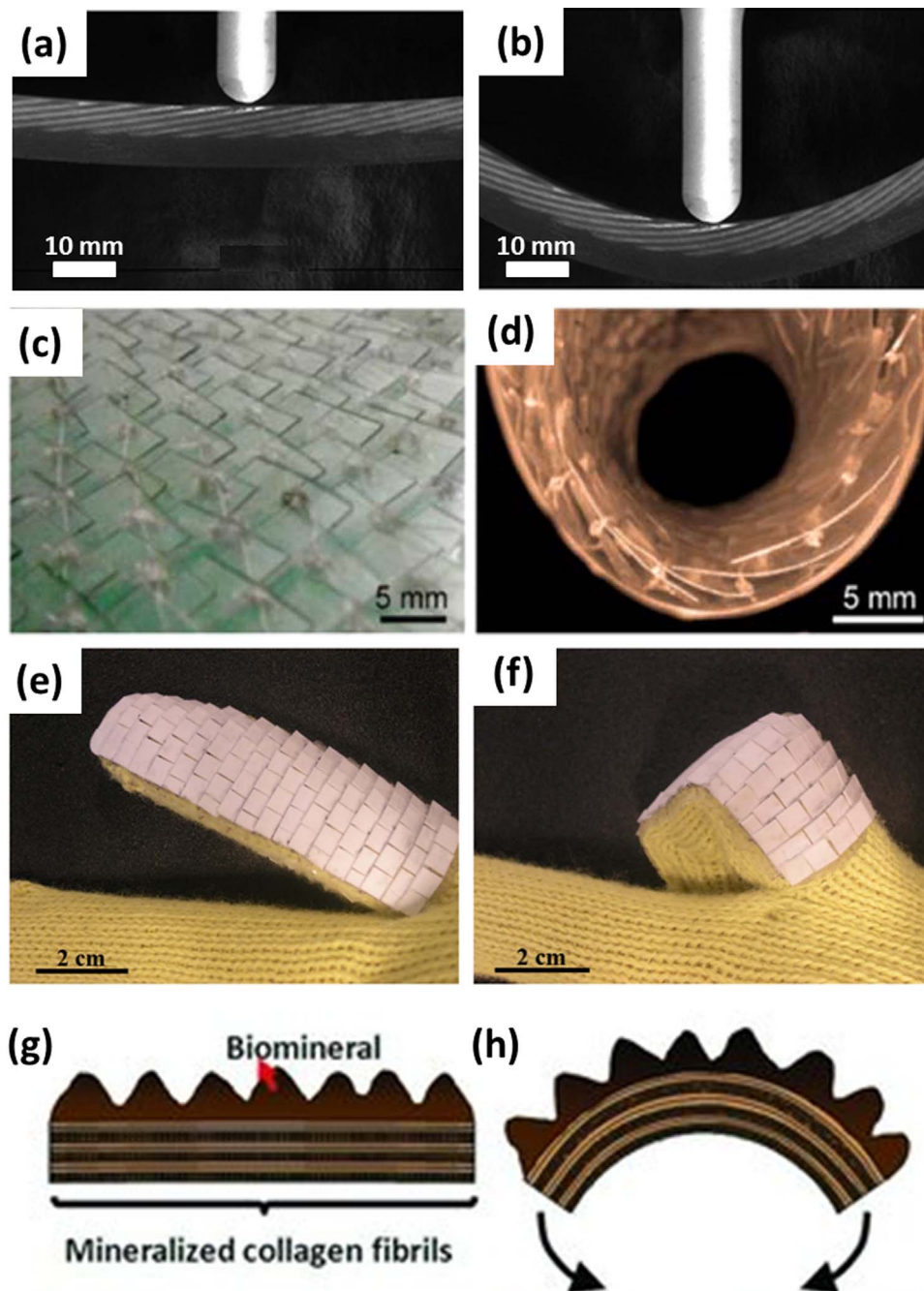


Fig. 18. Bioinspired armor designs. (a) and (b) Microstructured elasmoid scale armor produced by Rudykh et al. (2015) amplifies penetration resistance by a factor of 50 while reducing flexibility by less than a factor of 5. (c) and (d) A synthetic “fish skin” developed by Funk et al. (2015) combines a mesh or dermis-like layer and rigid protective scales. (e) and (f) Martini and Barthelet (2016b) produced this armor by stretching a soft substrate and affixing ceramic tiles, which leads to imbrication upon release. (g) and (h) Schematic of the flexing of the arapaima scale, which illustrates the concept of a “flexible ceramic”. Ridges minimize the tensile strains in the mineralized layer, preventing large cracks from forming during flexing. From Meyers et al. (2012).

Each type of scale has unique and fascinating features in its nano-, micro-, and meso-structure which lead to its capacity to prevent failure when under attack by either sharp teeth or crushing force of predators. If placed in alternative environments, each fish would be likely to suffer as the minimally overlapped gar scales may provide regions where a piranha's sharp teeth can penetrate into the fish's connective tissue and flesh, while the cycloid scales of the arapaima may not resist the powerful bite of the alligator. The understanding of these dermal armors and their effectiveness in protecting these three fish may inspire the production of novel designs for flexible body armor which provides superior safety and protection from physical threats.

Acknowledgements

This work was funded by the Multi-University Research Initiative Grant no. AFOSR-FA9550-15-1-0009 from the Air Force Office of Scientific Research to the University of California, Riverside, specifically through subcontracts to the University of California, San Diego and the University of California, Berkeley. We gratefully acknowledge Dianne and Gary Utery for generously providing a supply of alligator gar scales. Prof. P. Hastings and Mr. H.J. Walker from Scripps Institute of Oceanography generously provided us the scales of preserved coelacanths. Discussions with Prof. J. McKittrick, Dr. B. Gludovatz, and Dr. E.A. Zimmerman were helpful in the development of our ideas.

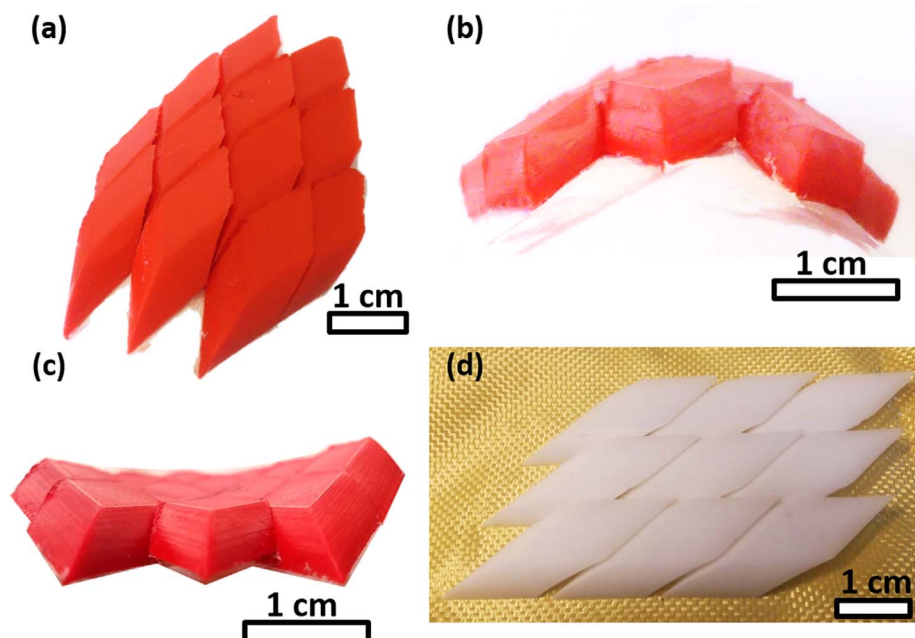


Fig. 19. 3D printed ABS and machined zirconia scales. (a) through (c) 3-D printed ABS and (d) machined zirconia scales were inspired from an idealized and symmetric ganoid scale geometry. They are designed to utilize key features of the alligator gar scales which lead to the scales' flexibility and effectiveness. This is achieved through matching radii of curvature on all sides of the scale which allows for hinge-like action between scales, as well as sufficient overlap to prevent gaps from forming between scales as they hinge. ABS scales were produced in order to refine the geometry and as a proof of concept, while zirconia scales were produced due to their strength and toughness as a technical ceramic.

We thank Mr. E. Hahn for the help revising the paper as well as contributions to sample preparation and microscopy, and Mr. E. Zamborsky at ARGEN for the manufacturing of ceramic scales.

References

- Allison, P.G., Chandler, M.Q., Rodriguez, R.I., Williams, B.A., Moser, R.D., Weiss, C.A., Poda, A.R., Lafferty, B.J., Kennedy, A.J., Seiter, J.M., Hodo, W.D., Cook, R.F., 2013. Mechanical properties and structure of the biological multilayered material system, *Atractosteus spatula* scales. *Acta Biomater.* 9 (2), 5289–5296.
- Bajaj, D., Arola, D.D., 2009. On the R-curve behavior of human tooth enamel. *Biomaterials* 30 (23–24), 4037–4046.
- Brainerd, E.L., 1994. Mechanical design of polypterid fish integument for energy-storage during recoil aspiration. *J. Zool.* 232, 7–19.
- Bruet, B.J.F., Song, J.H., Boyce, M.C., Ortiz, C., 2008. Materials design principles of ancient fish armour. *Nat. Mater.* 7 (9), 748–756.
- Chen, P.Y., McKittrick, J., Meyers, M.A., 2012. Biological materials: functional adaptations and bioinspired designs. *Progress. Mater. Sci.* 57 (8), 1492–1704.
- Chintapalli, R.K., Mirkhalaf, M., Dastjerdi, A.K., Barthelat, F., 2014. Fabrication, testing and modeling of a new flexible armor inspired from natural fish scales and osteoderms. *Bioinspir. Biomimetics* 9 (3), 036005.
- Daget, J., Gayet, M., Meunier, F.J., Sire, J.Y., 2001. Major discoveries on the dermal skeleton of fossil and Recent polypteriforms: a review. *Fish Fisheries* 2 (2), 113–124.
- Dastjerdi, A.K., Barthelat, F., 2015. Teleost fish scales amongst the toughest collagenous materials. *J. Mech. Behav. Biomed. Mater.* 52, 95–107.
- Deville, S., Saiz, E., Nalla, R.K., Tomsia, A.P., 2006. Freezing as a path to build complex composites. *Science* 311 (5760), 515–518.
- Erickson, G.M., Lappin, A.K., Vliet, K.A., 2003. The ontogeny of bite-force performance in American alligator (*Alligator mississippiensis*). *J. Zool.* 260, 317–327.
- Erickson, G.M., Lappin, A.K., Parker, T., Vliet, K.A., 2004. Comparison of bite-force performance between long-term captive and wild American alligators (*Alligator mississippiensis*). *J. Zool.* 262, 21–28.
- Ferrara, T.L., Clausen, P., Huber, D.R., McHenry, C.R., Peddemors, V., Wroe, S., 2011. Mechanics of biting in great white and sandtiger sharks. *J. Biomech.* 44 (3), 430–435.
- Fricke, H., Schauer, J., Hissmann, K., Kasang, L., Plante, R., 1991. Coelacanth *Latimeria Chalumnae* aggregates in caves: first observations on their resting habitat and social behavior. *Environ. Biol. Fishes* 30 (3), 281–285.
- Funk, N., Vera, M., Szewciw, L.J., Barthelat, F., Stoykovich, M.P., Vernerey, F.J., 2015. Bioinspired fabrication and characterization of a synthetic fish skin for the protection of soft. *Mater. ACS Appl. Mater. Interfaces* 7 (10), 5972–5983.
- Giraud, M.M., Castanet, J., Meunier, F.J., Bouligand, Y., 1978. The fibrous structure of coelacanth scales: a twisted 'plywood'. *Tissue Cell* 10 (4), 671–686.
- Goodrich, E.S., 1907. On the scales of fish, living and extinct, and their importance in classification. *Proc. Zool. Soc. Lond.* 77, 751–774.
- Helfman, G.S., Collette, B.B., Facey, D.E., 2009. *The Diversity Of Fishes-Biology, Evolution, and Ecology*. Wiley-Blackwell, Oxford, United Kingdom.
- Huber, D.R., Claes, J.M., Mallefet, J., Herrel, A., 2009. Is extreme bite performance associated with extreme morphologies in sharks? *Physiol. Biochem. Zool.* 82 (1), 20–28.
- Ji, B.H., Gao, H.J., 2010. Mechanical principles of biological nanocomposites. *Annu. Rev. Mater. Res.* Vol 40 (40), 77–100.
- Lin, Y.S., Wei, C.T., Olevsky, E.A., Meyers, M.A., 2011. Mechanical properties and the laminate structure of *Arapaima gigas* scales. *J. Mech. Behav. Biomed. Mater.* 4 (7), 1145–1156.
- Maciel, K.T., Carvalho, R.M., Ringle, R.D., Preston, C.D., Pashley, D.H., 1996. The effects of acetone, ethanol, HEMA, and air on the stiffness of human decalcified dentin matrix. *J. Dent. Res.* 75 (11), 1851–1858.
- Mara, K.R., Motta, P.J., Huber, D.R., 2010. Bite force and performance in the durophagous Bonnethead Shark, *Sphyrna tiburo*. *J. Exp. Zool. A Ecol. Genet. Physiol.* 313 (2), 95–105.
- Marino Cugno Garrano, A., La Rosa, G., Zhang, D., Niu, L.N., Tay, F.R., Majd, H., Arola, D., 2012. On the mechanical behavior of scales from *Cyprinus carpio*. *J. Mech. Behav. Biomed. Mater.* 7, 17–29.
- Martini, R., Barthelat, F., 2016a. Stability of hard plates on soft substrates and application to the design of bioinspired segmented armor. *J. Mech. Phys. Solids* 92, 195–209.
- Martini, R., Barthelat, F., 2016b. Stretch-and-release fabrication, testing and optimization of a flexible ceramic armor inspired from fish scales. *Bioinspir. Biomim.* 11 (6), 066001.
- Meyers, M.A., Chen, P.Y., Lin, A.Y.M., Seki, Y., 2008. Biological materials: structure and mechanical properties. *Progress. Mater. Sci.* 53 (1), 1–206.
- Meyers, M.A., Lin, Y.S., Olevsky, E.A., Chen, P.Y., 2012. Battle in the Amazon: arapaima versus Piranha. *Adv. Eng. Mater.* 14 (5), B279–B288.
- Munch, E., Launey, M.E., Alsem, D.H., Saiz, E., Tomsia, A.P., Ritchie, R.O., 2008. Tough, bio-inspired hybrid materials. *Science* 322 (5907), 1516–1520.
- Murcia, S., McConville, M., Li, G.H., Ossa, A., Arola, D., 2015. Temperature effects on the fracture resistance of scales from *Cyprinus carpio*. *Acta Biomater.* 14, 154–163.
- Murcia, S., Li, G.H., Yahyazadehfard, M., Sasser, M., Ossa, A., Arola, D., 2016. Effects of polar solvents on the mechanical behavior of fish scales. *Mater. Sci. Eng. C – Mater. Biol. Appl.* 61, 23–31.
- National Geographic "Arapaima." From (<http://environment.nationalgeographic.com/environment/freshwater/arapaima/>) (Retrieved 22.08.16).
- National Geographic, 2016b. (<http://environment.nationalgeographic.com/environment/freshwater/alligator-gar/>)
- Ørvig, T., 1957. Remarks on the vertebrate fauna of the Lower Upper Devonian of Escuminac Bay, P.Q., Canada, with special reference to the Porolepiform Crossopterygians. *Ark. Zool.* (10).
- Porter, M.M., Yeh, M., Strawson, J., Goehring, T., Lujan, S., Siripapasotorn, P., Meyers, M.A., McKittrick, J., 2012. Magnetic freeze casting inspired by nature. *Mater. Sci. Eng. A* 556, 741–750.
- Potts, S., 1998. *The American Alligator*. Capstone books, Mankato, Minnesota.
- Roux, G., 1942. The microscopic anatomy of the *Latimeria* scale. *S. Afr. J. Med. Sci.* 7, 1–18.
- Rudykh, S., Boyce, M.C., 2014. Analysis of elasmoid fish imbricated layered scale-tissue systems and their bio-inspired analogues at finite strains and bending. *IMA J. Appl. Math.* 79 (5), 830–847.

- Rudykh, S., Ortiz, C., Boyce, M.C., 2015. Flexibility and protection by design: imbricated hybrid microstructures of bio-inspired armor. *Soft Matter* 11 (13), 2547–2554.
- Sacks, M.S., Sun, W., 2003. Multiaxial mechanical behavior of biological materials. *Annu. Rev. Biomed. Eng.* 5, 251–284.
- Sherman, V.R., Yaraghi, N.A., Kisailus, D., Meyers, M.A., 2016. Microstructural and geometric influences in the protective scales of *Atractosteus spatula*. *J. R. Soc. Interface*, In Press.
- Sire, J.Y., Huyseune, A., 2003. Formation of dermal skeletal and dental tissues in fish: a comparative and evolutionary approach. *Biol. Rev.* 78 (2), 219–249.
- Sire, J.Y., Donoghue, P.C.J., Vickaryous, M.K., 2009. Origin and evolution of the integumentary skeleton in non-tetrapod vertebrates. *J. Anat.* 214 (4), 409–440.
- Smith, J.L.B., 1939. A living fish of Mesozoic type. *Nature* 143, 455–456.
- Smith, M.M., Miller, W.A., Hobdell, M.H., 1972. Structure of scales of *Latimeria-Chalumnae*. *J. Zool.* 167 (Aug), 501–509.
- Song, J., Ortiz, C., Boyce, M.C., 2011. Threat-protection mechanics of an armored fish. *J. Mech. Behav. Biomed. Mater.* 4 (5), 699–712.
- Sudo, S., Tsuyuki, K., Ito, Y., Ikohagi, T., 2002. A study on the surface shape of fish scales. *JSME Int. J. Ser. C – Mech. Syst. Mach. Elem. Manuf.* 45 (4), 1100–1105.
- Torres, F.G., Troncoso, O.P., Nakamatsu, J., Grande, C.J., Gomez, C.M., 2008. Characterization of the nanocomposite laminate structure occurring in fish scales from *Arapaima Gigas*. *Mater. Sci. Eng. C* 28 (8), 1276–1283.
- Vernerey, F.J., Barthelat, F., 2010. On the mechanics of fishscale structures. *Int. J. Solids Struct.* 47 (17), 2268–2275.
- Vernerey, F.J., Barthelat, F., 2014. Skin and scales of teleost fish: Simple structure but high performance and multiple functions. *J. Mech. Phys. Solids* 68, 66–76.
- Vickaryous, M.K., Sire, J.Y., 2009. The integumentary skeleton of tetrapods: origin, evolution, and development. *J. Anat.* 214 (4), 441–464.
- Wegst, U.G.K., Bai, H., Saiz, E., Tomsia, A.P., Ritchie, R.O., 2015. Bioinspired structural materials. *Nat. Mater.* 14 (1), 23–36.
- Yang, W., Gludovatz, B., Zimmermann, E.A., Bale, H.A., Ritchie, R.O., Meyers, M.A., 2013. Structure and fracture resistance of alligator gar (*Atractosteus spatula*) armored fish scales. *Acta Biomater.* 9 (4), 5876–5889.
- Yang, W., Sherman, V.R., Gludovatz, B., Mackey, M., Zimmermann, E.A., Chang, E.H., Schaible, E., Qin, Z., Buehler, M.J., Ritchie, R.O., Meyers, M.A., 2014. Protective role of *Arapaima gigas* fish scales: structure and mechanical behavior. *Acta Biomater.* 10 (8), 3599–3614.
- Zhu, D.J., Szewciw, L., Vernerey, F., Barthelat, F., 2013. Puncture resistance of the scaled skin from striped bass: collective mechanisms and inspiration for new flexible armor designs. *J. Mech. Behav. Biomed. Mater.* 24, 30–40.
- Zhu, D.J., Ortega, C.F., Motamedi, R., Szewciw, L., Vernerey, F., Barthelat, F., 2012. Structure and mechanical performance of a “Modern” Fish Scale. *Adv. Eng. Mater.* 14 (4), B185–B194.
- Zimmermann, E.A., Gludovatz, B., Schaible, E., Dave, N.K.N., Yang, W., Meyers, M.A., Ritchie, R.O., 2013. Mechanical adaptability of the Bouligand-type structure in natural dermal armour. *Nat. Commun.* 4, 2634.